ULTRASONIC TISSUE CHARACTERIZATION USING A SCANNING LASER ACOUSTIC MICROSCOPE AND AN IMAGE PROCESSOR

BY

DANIEL LAWRENCE COLBERT

B.S., UNIVERSITY OF ILLINOIS, 1984

THESIS

Submitted in partial fulfillment of the requirements
for the degree of Master of Science in Electrical Engineering
in the Graduate College of the
University of Illinois at Urbana-Champaign, 1986

Urbana, Illinois

ACKNOWLEDGEMENTS

I would like to thank Dr. William D. O'Brien, Jr. for giving me the opportunity to undertake this project. I would also like to thank him for his guidance and support, both technical and financial. Also, thanks to Dianne Steiger, Joe Cobb, and Wanda Elliott for their invaluable assistance along the way.

TABLE OF CONTENTS

CHAPTER PAGE

1 INTRODUCTION AND BACKGROUND 1

2 SYSTEM DESCRIPTIONS 6

3 METHODS 18

4 SERIES V RESULTS AND DISCUSSION 39

5 SUMMARY AND CONCLUSIONS 52

APPENDIX I: ULTRASONIC SPEED, ATTENUATION COEFFICIENT, AND HETEROGENEITY INDEX FOR SERIES V 54

REFERENCES 56

CHAPTER 1

INTRODUCTION AND BACKGROUND

1.1. Introduction

The 100 MHz Scanning Laser Acoustic Microscope (SLAM) has proven to be a reliable system with which to measure the ultrasonic properties of different tissues. A previous study used the SLAM system to measure acoustic speed and attenuation coefficient in wound tissue extracted from dogs [1]. The two major conclusions drawn from this study were that the changes in the mechanical properties (tensile strength) and in the collagen concentration during wound healing were found to be highly correlated with the acoustic parameters of speed and attenuation, and also, a heterogeneity index, derived from the speed measurement, was neither sensitive nor accurate enough to reflect changes in the wound healing process. As a result, no solid conclusions could be drawn about whether or not heterogeneity in the wound increases as a function of age. However, the study did confirm that ultrasound can be used to evaluate wound status [2].

From the results of the previous study [1], which consisted of series III and series IV dogs, a series V study was undertaken. The specific objectives of the series V experiments were:

1. To determine the ultrasonic speed and attenuation coefficient in the wound and adjacent skin as a function of wound age.

2. To determine the ultrasonic speed and attenuation coefficient in normal, unwounded skin as a function of specimen location.
3. To quantitatively determine a significant measure of acoustic heterogeneity in the skin and wound as a function of wound age using an image processor.

The series V study and its results will be the subject of this report. Chapter 2 describes the SLAM, its data acquisition system, and the system 575 image processor (International Imaging System, Inc.). The experimental methods used in this study, including specimen preparation, acquisition of biochemical data, and processing of the SLAM data are discussed in Chapter 3. Results of the series V experiment are presented in Chapter 4. Conclusions and a discussion of how well the series V results correlate with the earlier study are contained in Chapter 5.

1.2. Background

Skin is a very high collagen content tissue, with collagen making up 70% of the dry weight [3]. When an incision is made in skin, the collagen fibers are cut and the skin's tensile strength falls to zero. As healing occurs, collagen is replaced and restructured. Since the amount, structure, and arrangement of collagen fibers are the primary contributors to tensile strength the healing process restores tensile strength in the wounded skin [4]. Consequently, collagen, in addition to being one of the most important elements involved in the wound healing

process, is regarded as the most important parameter in assessing wound status [5].

The wound healing process can be divided into three phases based on changes which occur in wound collagen content. Phase one is the lag or inflammatory phase. Lasting approximately four to six days after wounding occurs, it is associated with the removal of cellular debris and with infection control [5]. During this first phase the wound shows no increase in tensile strength. The second phase is called the logarithmic, fibroplastic, or proliferative phase. During this stage, which lasts from six to 30 days post wounding, there is a large increase in collagen synthesis and deposition of new collagen in the wound tissue. Tensile strength exhibits the largest increase during this phase. The remodeling or maturation phase occurs last. In this stage the rate of collagen synthesis decreases but tensile strength continues to increase. This phenomenon is caused by the existing fibers increasing in size and undergoing structural changes such as cross-linking [6]. As collagen becomes cross-linked, its solubility decreases and strong acid solutions must be used to dissolve the collagen. Consequently, acid solubility is a good measure of the amount of cross-linking present.

In addition to playing a major role in the wound healing process, collagen is also an important contributor to the ultrasonic propagation properties in most tissues [7]. This is because the acoustic characteristics of collagen are very different from those of globular proteins. For example, Young's modulus for collagen is approximately 1000 times greater than it is for most

soft tissues, and the density of collagen is also greater [8,9]. Since ultrasonic speed and acoustic impedance are directly related to the elastic modulus, collagen is thought to be the major contributor to sound propagation in tissues [10,11]. The arrangement or orientation of tissue collagen also has an effect on its acoustic properties. Called acoustic anisotropy, this phenomenon has been observed in muscle [3]. Water content itself does not really affect the absorption properties of tissue, but since it has the effect of diluting tissue protein concentration it probably does affect the acoustic properties.

Studies have been done which support the notion that it is primarily the tissue proteins and collagen, in particular, which determine the acoustic propagation properties in most tissues. The series III and series IV studies done recently [1] examined the biochemical and ultrasonic properties in wound tissue, as well as the various correlations between the two. In general, the results supported the existing theories. The ultrasonic speed and attenuation coefficient, were both significantly correlated with tissue water content and total collagen content. The ultrasound data alone showed that ultrasonic speed and attenuation coefficient were consistently lower in the wound than in the skin and increased with wound age. Also, section type (orientation) had no effect on speed, attenuation, or heterogeneity. The biochemical data also turned out as expected. The total collagen content in the wound was lower than in skin for all ages, and increased with wound age. The acid soluble collagen was the same in the wound and skin until day 14 and then increased in the

wound. By day 50, the acid soluble collagen was 3 - 4 times higher in the wound than in the skin. Clearly, ultrasonic analysis of wound tissue is a valid method of assessing changes in the wound healing process and correlates very well categorizing with the more traditional biochemical methods of the wound healing process.

CHAPTER 2

SYSTEM DESCRIPTIONS

The 100 MHz Scanning Laser Acoustic Microscopy (SLAM) with its data acquisition system, and the International Imaging Systems (IIS) system 575 image processor were the two systems used for data collection and analysis. Also, a statistical package available on the University of Illinois Cyber Computer was used for an analysis of variance on the data. This chapter will briefly cover the set-up and operating principles of the SLAM, the SLAM data acquisition system, and the IIS image processor.

2.1. Scanning Laser Acoustic Microscope

The operating principles of the SLAM have been thoroughly described elsewhere [12], and will only be summarized here. The Sonomicroscope 100 is an analytical instrument which produces magnified images of objects using high frequency (100 MHz) acoustic waves. Figure 1 shows a diagram of the system. Acoustic energy is transmitted into the sample through a fused silien stage using a piezoelectric transducer. After passing through the sample the sound is detected by a rapidly scanning, focused laser beam. The 2 mm by 3 mm image thus formed is called an acoustic micrograph, and the imaging technique is called acoustic microscopy.

Using the SLAM, a specimen is viewed by placing it on a stage and covering it with a glass coverslip, the bottom surface of which has been plated with a semireflective gold film. It is

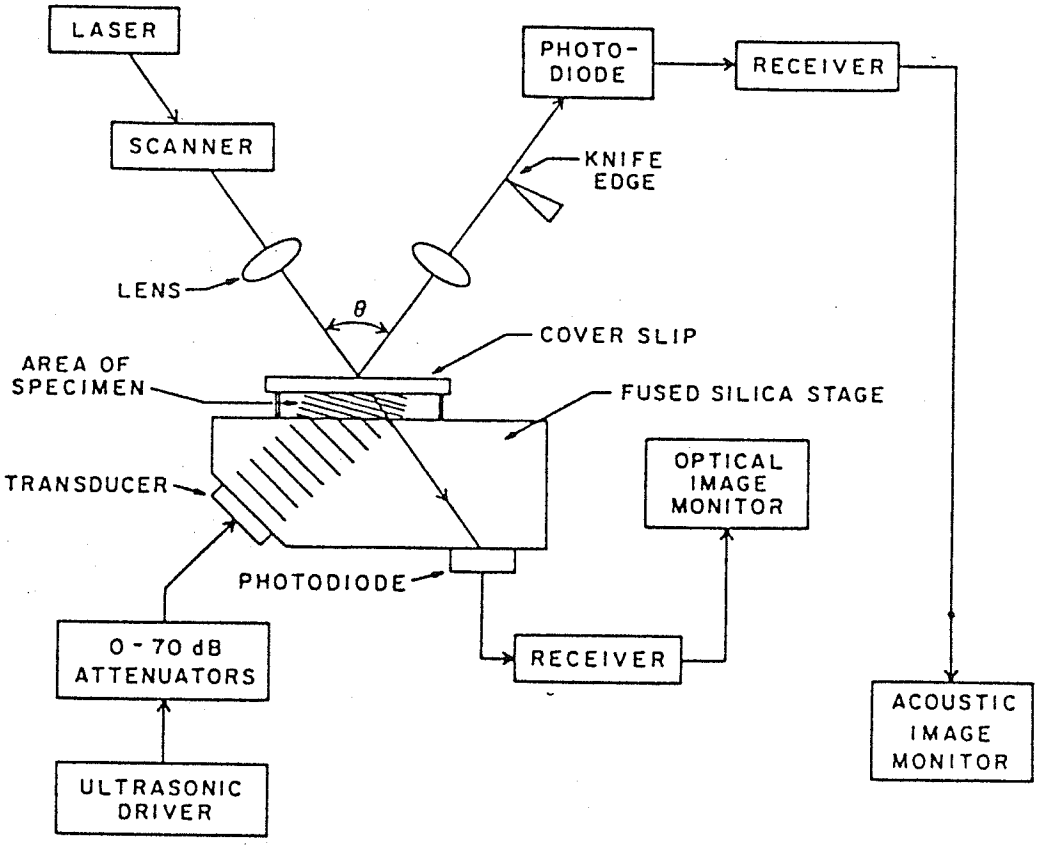

Figure 1 - Block diagram of the SLAM.

then insonified with plane acoustic waves and illuminated with laser light. The optically reflective surface of the coverslip becomes distorted in proportion to the localized sound pressure. These distortions are dynamic in that the pressure wave is periodic and the mirror displacements accurately follow the wave amplitude and phase. The coverslip surface then is an optical phase replica of the sound field at every instant of time and the laser is used to measure the degree of regional distortion.

A laser beam incident upon the coverslip surface is reflected at an angle equal to the incident angle. When the surface is titled by an amount proportional to the sound pressure, the reflected light is angularly modulated (spatially). If all the reflected light is captured by a photodiode, its electrical output signal will be a DC level only, because the light power reaching the detector will not change as a function of the angle. However, if part of the beam is blocked by a knife edge, then the amount of light reaching the photodiode will depend upon the instantaneous angular position of the beam. As a result, the electrical signal output will now consist of a DC component plus a small 100 MHz AC term coherent with the acoustic amplitude. In this way knife edge detection forms the basis of the rapid detection of sound and the display of acoustic images.

Three types of images can be produced by the SLAM: an optical image, an acoustic image, or an interference image. An example of each is shown in Figure 2. The optical image is obtained by collecting the portion of light transmitted through both the sample and coverslip with photodiode. The optical image

(a)

(b)

(c)

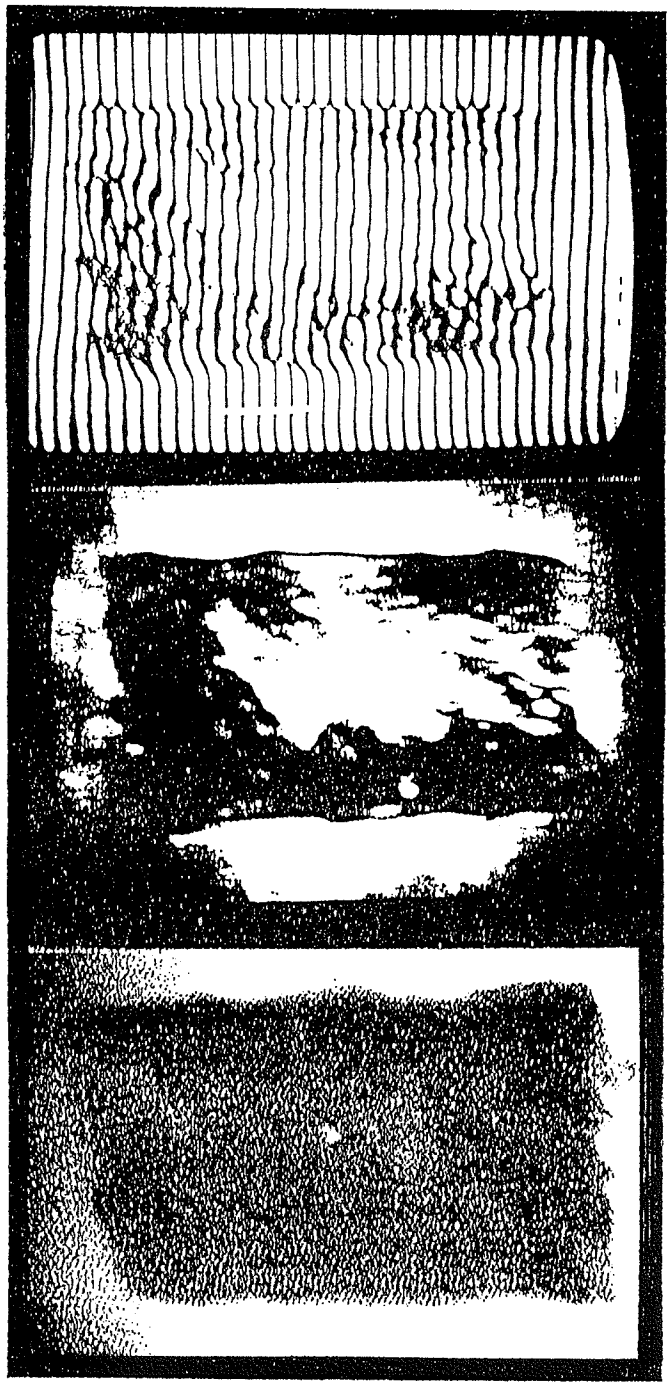

Figure 2 - (a) interference, (b) acoustic amplitude, and (c) optical SLAM images for a 100 μm section with a 20 day old wound.

is useful in positioning the specimen properly on the stage. To produce an acoustic image, the laser must be scanned in a raster pattern across the surface of the coverslip. The scanning technique is based upon the use of an acoust-optical diffraction cell with a frame rate identical to that of standard TV 30 frames per second. Acoustic attenuation can then be determined by quantifying the brightness levels of the acoustic image on the CRT display.

The acoustic interference image, or interferogram, is produced by electronically adding a reference signal, which is phased coherent with the transmitted acoustic wave before passing through the specimen, to the received signal. A series of regularly spaced fringe lines (alternating light and dark vertical bands), caused by mutual interference of the reference signal and the acoustic signal incident on the coverslip surface, will occur. A change in phase due to a change in ultrasonic speed will cause the fringes to bend to the right if the ultrasonic speed is increasing and to the left if the speed is decreasing. The speed of sound in an unknown specimen can be determined by the amount of horizontal shift in the fringe lines when passing from reference medium of known ultrasonic speed into the specimen of interest.

A basic understanding of acoustic micrographs in terms of specific material properties may be obtained by considering what happens to acoustic waves as they propagate through a material. Within a sample the sound is scattered and absorbed according to the internal elastic microstructure. In inhomogeneous materials

sound waves will be reflected and/or refracted at internal boundaries where the elastic properties change. This process diverts energy away from the insonifying beam. Inhomogeneities somewhat larger in size than an acoustic wavelength, 20 microns in this system, will be individually resolved and appear on the micrograph. When the inhomogeneities are comparable to or smaller than an acoustic wavelength, attenuation of the acoustic beam is due to scattering. An additional source of acoustic attenuation is termed absorption. This occurs in all materials, and is a dominant mode of loss in liquids, polymers and biological tissues. Absorption refers to losses arising from the conversion of acoustic energy to other energy forms such as viscous damping for frictional loss. By measuring the speed of sound and the acoustic attenuation in a specimen, its localized (regional) variations in elasticity and density can be quantitatively determined. The next section describes the data acquisition system which allows quantitative determination of the ultrasonic parameters mentioned above.

2.2. SLAM Data Acquisition System

A block diagram of the system used for data acquisition is shown in Figure 3. A short description of the system and its features follow.

The system, which is controlled by a Z-80 microprocessor, includes two serial ports. One port is connected to the VAX 11/730 for file and data transfer, and the other port is connected to a terminal for data entry and program control. The

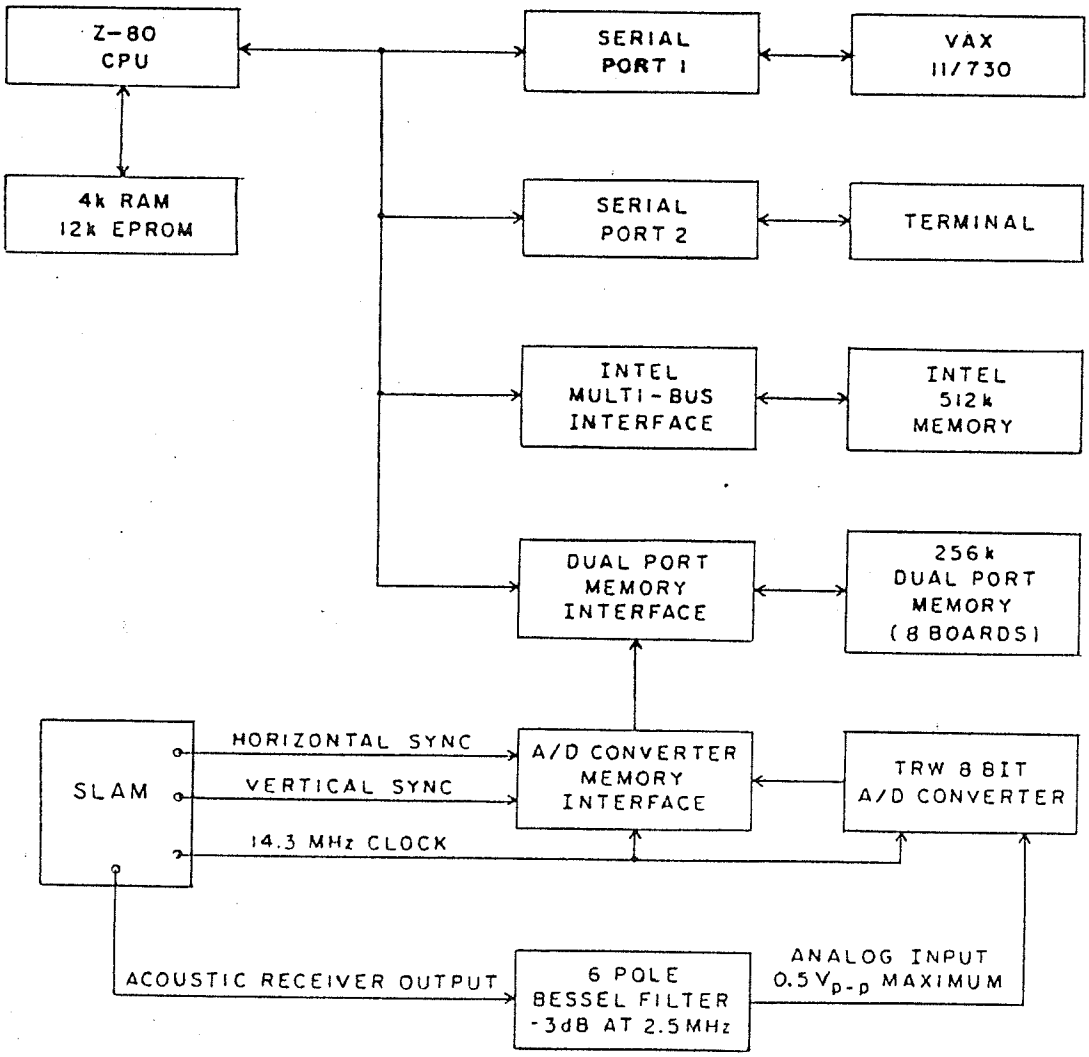

Figure 3 - Block diagram of the SLAM data acquisition system.

mother board has a 12 K eprom which contains the system monitor as well as a BASIC interpreter program. This BASIC interpreter enables the user to compile and execute BASIC programs on the system.

Two types of memory are used in the system, high speed dual port memory and Intel^{R} multibus memory. The high speed dual port memory allows for storage of up to 256 K bytes of data. It can be accessed either by the analog-to-digital converter for storage of SLAM image data, or by the Z-80 microprocessor for data manipulation and analysis. An additional 512 K bytes of Intel^{R} multibus memory is available for data storage and allows for frame averaging. Frame averaging is accomplished by adding the digitized image data stored in the dual port memory into the Intel^{R} memory as successive frames are imaged and stored in the dual port memory. Averaging occurs in the Intel^{R} memory after the desired number of frames have been digitized and added to the data of a previous frame or frames in about 4 seconds. This represents a substantial improvement in both speed and sensitivity over the previous set up [13,14]. One frame of the SLAM image is digitized into 768 points horizontally by 255 points vertically for a total of 195,840 bytes. An entire frame can be digitized and stored in the dual port memory in about 16 ms.

A TRW TDC 1007PCB 30 MHz, 8-bit A/D converter is used to digitize the SLAM data. Before being fed into the A/D converter the acoustic receiver output is low-pass filtered in order to eliminate the effects of aliasing. A six pole Bessel filter with a -3 dB point of 2.5 MHz was chosen because of its linear

phase response. The A/D converter's 14.3 MHz clock signal and the frame horizontal and vertical sync signals are taken directly from the SLAM.

2.3. System 575 Image Processor

The system 575 drives a library of functions for classifying, analyzing, enhancing, and performing various processes upon images using IIS's model 75 image processing system. An executive program called the command interpreter (CI) coordinates the running of applications functions on the system 575. The command interpreter initializes and maintains a large buffer (16,384 words) called the function communication block (FCB). The FCB is then used to pass information to each function that is run under the system 575.

System 575 software has been divided into several levels for modularity. The highest level applications programs are written in machine-independent Fortran to keep the system transportable. As the executive program of the system, the CI Parses and attempts to execute each command string entered by the user. It does this by calling a software "driver" which then calls a "primitive" where the particular image processing is performed. The primitive will in turn call several low-level routines called "intrinsics" which perform image and display I/O, handle interrupts, and perform image reads and writes. The terms "driver" and "primitive" are unfortunate in that they usually have a different connotation outside of IIS.

Driver is not meant to be an I/O driver or device handler in

the usual sense. Rather, its main functions are to check for the correct number of inputs and outputs for the function being called, open and close the inputs and/or output images, check file types, prompt for and define function parameters, and then go on to call the primitive. Primitives are not the lower-level routines dealing with I/O, interrupts, bit and byte manipulation and the like. These operations are handled by the intrinsics. Rather, primitives are each called by a specific driver. Inside each primitive is the heart of the particular image processing algorithm that the user wishes to perform. The primitive performs no terminal or disk I/O. Instead, primitives accomplish their image processing objectives by successively calling the proper intrinsics. As mentioned above, the intrinsics are those low-level routines that interface with the model 75, perform device and image I/O, handle error reporting, perform bit and byte manipulations and other chores.

The system 575 is designed as a general purpose image processing system that sets up a "friendly interface" between the user, the host computer's operating system, and the model 75 image processing hardware. In this case the system 575 is being supported on the DEC RSX-11M operating system. The system 575 is essentially a specialized operating system that takes advantage of the capabilities of the standard host computer operating system. Once the system is invoked, the user is elevated to an operating level unencumbered by programming and hardware details.

The system 575 provides two distinct storage media: refresh

memory and disk. Each medium supports some set of three distinct data types: unsigned 8-bit; signed 16-bit, 2's complement data; 32-bit floating point data. Since model 75 refresh memory is limited to a maximum of eight bits per channel, display images must be of byte data type. Disk is not limited in this way and the system 575 provides for the appropriate data type conversions where necessary.

An image is stored in refresh memory using the display command, which moves the data from the disk to the model 75. An upper limit exists on the number of images that can be stored in refresh memory. A first in, first out method is used to allocate this memory. In order to facilitate the handling of a large number of images, an image directory is utilized which contains all the data pertaining to each image known to the system. This directory is known as the "image name directory" and is maintained by the CI.

Digital images, as supported by the system 575 are essentially three-dimensional arrays of pixel intensities. The three dimensions of these images are expressed as sample, lines, and bands. Sample is the name applied to the X or horizontal pixel direction and line is the name used to describe the Y or vertical pixel direction. Bands are differentiated in that they generally contain spectral, temporal, or other data rather than spatial information. All the bands of an image represent the same physical location, but contain different information about that location. This information can be differing wavelengths of

the electromagnetic spectrum, elevation, depth of penetration, or different times, depending on the application.

Each channel of the system is capable of storing up to 512 bytes of data. This limits normal display resident images in the samples and lines dimensions to 54123 pixels, although larger images can be explored using the roam function. Several methods of reducing the size of a disk or tape image, such as subsampling, subsectioning, and subbanding, are also provided by the system 575. Images smaller than 512 by 512 are automatically centered both in refresh memory and on the monitor.

CHAPTER 3

METHODS

3.1. Tissue Preparation

Details of the wounding procedure, specimen excision, and specimen preparation have been published previously [15] and will only be summarized in this section. A more thorough discussion of the tissue handling techniques used to prepare the specimen for investigation with the SLAM will be presented.

The series V experiments, results of which are presented in this thesis, involved measurements on two dogs with wound ages of 9, 20, 33, 49, 75, and 99 days from each dog. Incisional skin wounds were made on the back of the dogs parallel to the vertebrae. Blocks of tissue containing the wound and adjacent skin, with the wound located in the center, were excised and mounted with Ames OCT compound on 2 cm diameter circular pieces of cork. An unwounded area of skin located some distance from the wound was also cut for each wound age to provide a control. Within 5 minutes of excision the samples were frozen in liquid nitrogen, sealed in plastic bags, and transported on dry ice. The skin specimens were prepared at the University of Washington in Seattle and were shipped to the Bioacoustics Research Laboratory where they were stored in a -70^{o}C Forma-scientific freezer until analyzed.

At the time of ultrasonic analysis, the tissue specimens were removed from the -70°C freezer, and the corks to which they had been attached were mounted on the object disk of a Lipshaw Cryostat with Tissue-Tek^{R} OCT compound. The object disk was then mounted in the Cryostat, which was maintained at -35°C, and approximately 50 to 100 m of the top surface of the specimen was cut off and discarded in order to provide a flat, even surface for subsequent sections. For each specimen frozen sections of 50 or 75 μm, 100 μm, and 150 μm in thickness were cut, transferred to a glass slide, and covered with normal saline. The 150 μm sample was always cut first and the 50 or 75 μm sample was cut last. The uncertainty in the thickness of the sections obtained using the Cryostat is approximately ± 10%.

The specimens were coded so that the wound age was not known at the time of acoustical analysis. For each wound age, a perpendicular section (sectioning perpendicular to the skin surface) was provided. Figure 4 shows the orientation of the wound, skin surface, and plane of sectioning for a perpendicular section.

If the wound area in a specimen was not clearly visible, a dissecting scope was used to aid in locating the area. In some cases, it was necessary to stain a section of the specimen with toluidine blue dye in order to locate the wound. Dying caused the wound area to appear as a darker blue strip than the surrounding skin. The stained section was subsequently used as a guide in locating the wound area in the sections used for acoustic analysis. After the wound was located, each section was trimmed to a size 2.5 to 3.0 mm horizontally by 1.5 to 2.0 mm

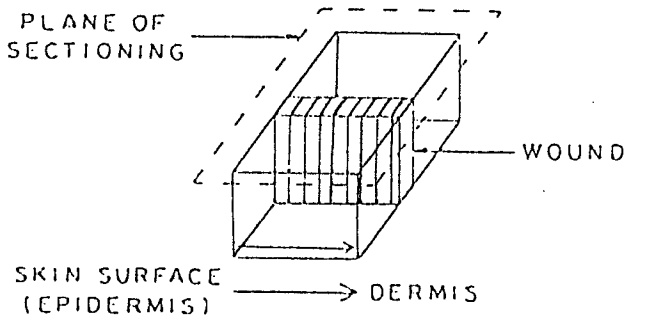

Figure 4 - Diagram of a perpendicular tissue section indicating the skin surface, the location of the wound, and the plane of sectioning.

vertically in order to fit within the field of view of the SLAM. When the width of the wound area was less than 0.5 mm, the sections were trimmed so that the wound was in the center with about 0.5 mm of skin on either side. In cases where the wound area was wider, sections were trimmed so that they were about 1/2 skin and 1/2 wound. In all cases the skin-wound interface was in the horizontal direction. Sections were gently transferred from the glass slide to the microscope stage by floating them on a layer of saline to prevent stretching or breaking. The total time for cutting and analyzing one section using the SLAM was about 30 minutes.

3.2. Ultrasonic Attenuation Coefficient

The ultrasonic attenuation coefficient is an important tissue characterization property which represents the decrease in energy of the sound wave when it propagates through a material. The attenuation includes both absorption and scattering of the insonifying beam. Absorption represents the loss of energy into heat within the specimen, while scattering is a redirection of the energy due to the inhomogeneities of the specimen and includes reflection, refraction, and diffraction.

One of the earliest attenuation coefficient measurement techniques relied upon the operator's subjective opinion of the overall brightness on the monitor of the interference mode image [16]. The insertion loss was determined by visually examining the interferogram image while reducing the transducer's driving voltage with a calibrated electrical attenuator located between the

ultrasonic driver and transducer and assessing when the interference lines disappeared. The process was repeated with and without the specimen in place, and the difference in readings of the calibrated attenuator gave the insertion loss. This procedure relied greatly on operator judgement and consequently each measurement had an uncertainty of $\pm$ 3 dB. The same technique has been evaluated using the acoustic image as well. Light and dark areas in the acoustic image correspond to areas with low or high ultrasonic attenuation levels in the object, respectively. However, it is difficult to use the acoustic image because the system is not linear, the signal-to-noise (S/N) ratio is low, and the acoustic illumination is not uniform.

In response to the problems inherent with each of these procedures, a new insertion loss technique, utilizing the data acquisition system and the acoustic image, was developed [1]. This technique involves the comparison of two received signal amplitudes, one with and the other without a specimen of known thickness inserted in the sound path. The insertion loss values plotted versus a range of thicknesses of the same specimen gives a line. The slope of this line yields the attenuation coefficient, and the intercept represents the attenuation due to reflective losses. Figure 5 shows a typical example. Since this method uses the acoustic image, the principal technical difficulties in measuring the attenuation coefficient with the SLAM are its nonlinearity, low S/N ratio, nonuniform illumination of the specimen, and raster signal reference level variation with the signal level. System noise has a Gaussian distribution and so

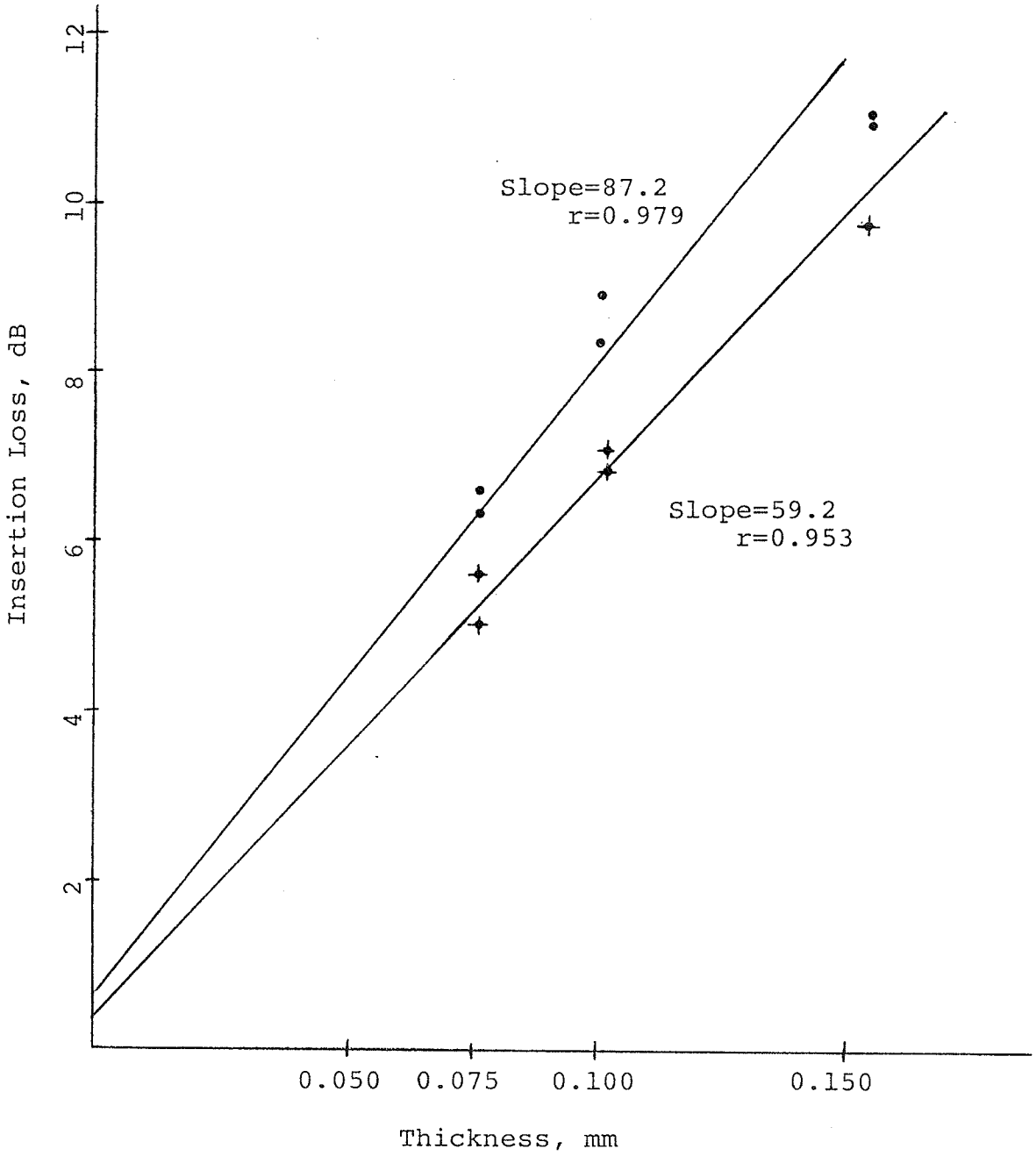

Figure 5 - Insertion loss versus thickness curves for skin (●) and wound (✦) areas in a tissue section with a 49 day old wound.

the system S/N ratio may be improved by signal averaging [17]. To avoid the problem of nonuniformity of the image, a small subarea of the image where the field is essentially uniform is used to determine insertion loss. The reference level for each raster line is measured and subtracted from the signal level to account for the nonconstant reference level. To measure the system linearity, a thick layer of saline was placed between the stage and coverslip. The receiver gain was then adjusted to use the full range of the A/D converter. The decrease of the acoustic image video signal was recorded as a function of electrical attenuation inserted between the ultrasonic drive and transducer. Both the slope and correlation coefficient are very close to 1, indicating the system is nearly linear [16].

An area 96 pixels horizontally by 32 pixels vertically, about 400 x 250 μm, near the center of the acoustic image was chosen as the imaging area. The SLAM was adjusted so that the brightest, most uniform area of the image was located at the imaging area. To insure that the imaging area remained fixed, the specimens to be examined were placed on a thin plastic sheet coupled to the SLAM stage with water. The plastic sheet allowed samples to be easily moved around on the stage without disturbing the position of the measurement area. Examination of the plastic material has shown that it does not affect the illumination uniformity of the sound field. To account for the change of the reference level with varying signal level, the reference level and appropriate signal level are captured from the same raster line. The raster line reference level was determined from 8 - 10

samples of the backtrace and subtracted from the signal levels in the imaging area.

The BASIC program controls digitization of the image area and calculation of an average, reference corrected value for the area. The BASIC program can also be adjusted to repeat this operation a selected number of times, calculated the average of all the image area averages, convert these values to decibels, and display the values on the screen. The voltage value for a subimage is calculated in a 3072 point array according to

$$V = 10 \text{ Log} \left\{ 1/n \sum_{1}^{n} [(1/3072) \sum_{i=y}^{y+31} \sum_{j=x}^{x+95} (v_{ij} - r_i)] \right\} \quad (1)$$

where V = the average of the image area averages expressed in dB,

n = the number of times the imaging area is averaged,

i = image row index,

j = image column index,

y = starting row number of the imaging area,

x = starting column number of the imaging area,

v_{ij} = digitized value of the pixel at the i^{th} row and j^{th} column, and

r_i = average reference level of the i^{th} row raster line.

To determine the insertion loss for any specimen, the specimen and coverslip are placed on the plastic sheet along with a thin layer of normal saline, $\leq$ 25 μm, with a coverslip. The SLAM is then adjusted using the saline to optimize the imaging area for brightness and uniformity. Several values of V are recorded for the saline layer. Finally, the plastic sheet is moved so

that the specimen to be examined is in the imaging are, and several values of V are recorded for the specimen. An insertion loss value in dB for each value of V recorded for the specimen is determined using

$$IL = V_s - V_r$$

where V_r = average of the V values recorded for the saline reference layer, and

V_s = value of V recorded for the specimen.

The uncertainty of the insertion loss values was determined by measuring the variation in V obtained for layers of saline with varying amounts of electrical attenuation inserted. Since saline is a homogengeous medium, and the imaging area was not changed throughout the measurement, the variations in the values obtained are solely due to electrical noise, variation in the power of the transducer or laser, and other unknown variations in the system. Twenty values were recorded for each of the four different levels of attenuation and the mean and standard deviation of each level was calculated. The uncertainty in V, calculated as two standard deviations of the mean was $\pm$ 0.12 dB. Since insertion loss is determined by subtracting one V value from another, the uncertainty in the insertion loss is found using

$$\Delta IL = \sqrt{V_s^2 + V_r^2}$$

where Δ refers to the uncertainty in IL. Using $\pm$ 0.12 dB as the uncertainty for V_s and V_r gives an uncertainty for the IL of $\pm$ 0.17 dB.

The linearity and accuracy of the insertion loss technique were evaluated by using precision electrical attenuators to decrease the ultrasonic energy transmitted to the stage. These attenuators, which reduce the driving voltage of the transducer are located between the ultrasonic driver and transducer. An impedance mismatch between the ultrasonic driver output and electrical attenuators causes the driver output power to change whenever the attenuators are switched into the system. This mismatch problem was overcome by adding 20 to 40 dB of baseline attenuation. Unfortunately, this causes a significant reduction in the baseline power level, which also significantly decreases the S/N ratio. This problem was avoided by switching 40 dB of attenuation into the system and adding a wideband power amplifier between the attenuator output and the transducer input. Using this set up, it has been previously demonstrated that insertion loss versus inserted attenuation is linear and that the insertion loss technique is very accurate [1].

The attenuation coefficient was determined for the skin specimens by first determining the insertion loss for three thicknesses (75, 100, and 150 μm) of each specimen as described earlier. Three to five separate insertion values from different areas of the specimen were obtained for both the wound and adjacent skin areas in each specimen. The slope of the best fit line, determined from a linear least squares analysis, yields the attenuation coefficient in dB/mm. The spread of insertion loss values for a given thickness is due to specimen heterogeneity, and not uncertainty in insertion loss, because each IL value rep-

resents a different area of the specimen. The uncertainty in the attenuation coefficient is due to both the uncertainty in IL and to the uncertainty in specimen thickness. An earlier study verified the accuracy of the method for determining the attenuation coefficient and also determined that the uncertainty in the measured value is quite large [1]. For skin samples with a thickness uncertainty of ± 10%, the uncertainty in the attenuation coefficient is approximately 35%.

3.3. Determination of Ultrasonic Speed

The vertical interference lines of the interferogram represent equal phase wavefronts after the sound wave has passed through the specimen. This spatial map of the phase information of the acoustic wave yields the speed of sound in the specimen shown in Fig. 6. A specimen with a speed greater than that of the surrounding reference medium (saline) has been positioned horizontally across the center of the interferogram. It is evident from the figure that the interference lines shift to the right as they pass from the reference medium into the specimen. Each interferogram consists of approximately 37 interference lines spaced at intervals of 80 μm.

If both the speed of sound in the reference medium and the thickness of the specimen are known, the speed of sound in the specimen can be determined from the amount of shift in the fringe lines. The equation given below is used to determine velocity.

$$c_x = (c_o/\sin\theta_o) \sin\left\{\tan^{-1}\left[(1/\tan\theta_o) - N_o/T \sin\theta_o\right]^{-1}\right\} \qquad (2)$$

(a)

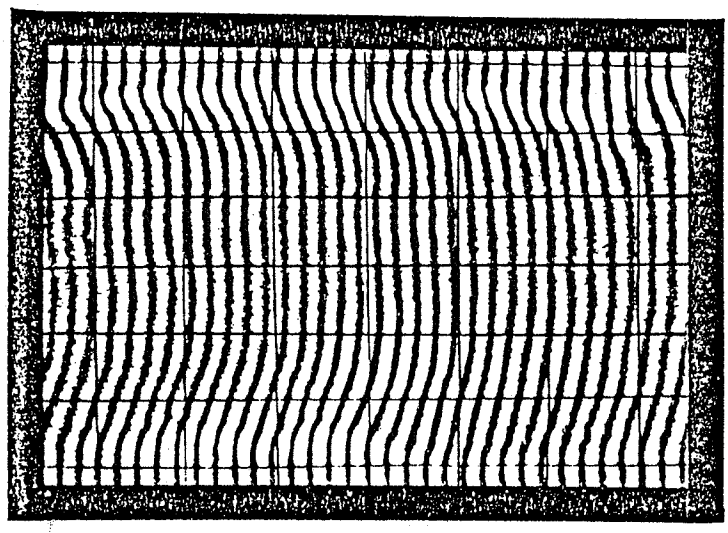

(b)

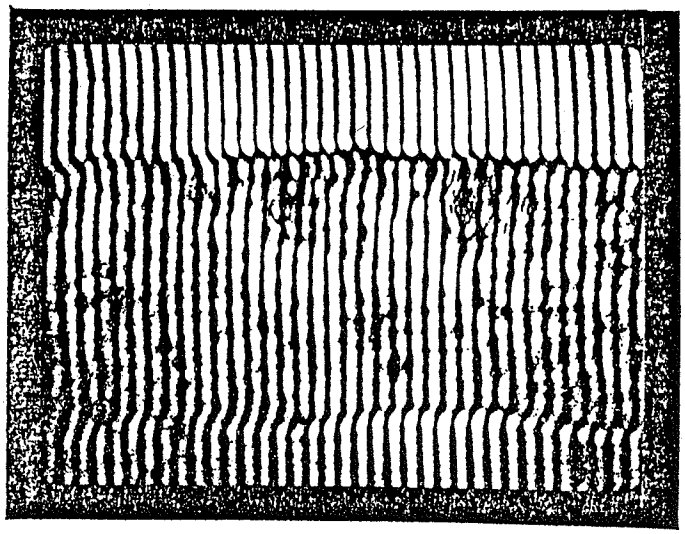

Figure 6 - SLAM interference images for a homogeneous liver specimen (a) and a heterogeneous skin specimen (b).

where cx = speed of sound in the specimen of interest,

c_o = speed of sound in the reference medium

θ_o = angle of sound (from the normal) in the reference medium,

N = normalized fringe shift,

λ_o = wavelength of sound in the reference medium and equals c_o/frequency of sound (100 MHz),

T = specimen thickness.

The only unknown in the above equation is N, the normalized fringe shift. N is determined by dividing the horizontal distance that the fringe has shifted from the reference medium by the horizontal distance between the interference lines.

The first method of finding N involved directly measuring the necessary horizontal distances from either the SLAM monitor or from a photograph of the monitor. However, this procedure only yielded a single ultrasonic velocity for each interference line and the precision of N was only within 0.1 of a fringe.

A more recent method determined speed by using an automated spatial domain technique which allowed for computer enhancement of the interferogram. A correlator receiver was used to compare the signal of the raster line with a stored replica of the ideal cross section of an interference line maxima. At locations of maximum correlation, the center of each of the interference lines for that raster line is noted. This enhancement process proceeds for all 255 raster lines, for which there are about 39 interference line positions noted per raster line. A single interference line then consists of 255 data points and yields up to 155 indi-

vidual normalized fringe shift data points. The reason each line only yields 155 points is that the specimen is prepared on the stage such that the top and bottom 50 data points of each line lie within the reference medium. At this point a line following and smoothing algorithm was implemented. The process produced up to 155 velocity data points for each interference line with the precision of N within 0.03 of a fringe. With this method, the precision is mainly limited due to quantization error, instead of operator error as before. A major requirement for this method to be successful is that the tissue must be relatively homogeneous. If the specimen is too heterogeneous a fringe shift ambiguity problem develops within the specimen. As a result, the spatial domain technique is not very well suited for assessing the velocity distribution of specimens such as dog skin which is very heterogeneous.

The spatial frequency domain technique (SFDT) was devised [21] to deal with heterogeneous specimens. This technique, with some modifications made in a previous work [22], was used to determine the speed of sound in this study. The SFDT determines the normalized fringe shift, N, in the frequency domain rather than in the spatial domain.

The Fourier Transform of a horizontal raster line is its spatial frequency spectrum. If the phase components of the Fourier transforms of two raster signals, one shifted relative to the other, are evaluated at the frequency at which the spectrum is a maximum, the difference in their phases, $\Delta\phi(\xi_o)$, is given by

$$\Delta\phi(\xi_o) = 2\pi y_o/\lambda_y = 2\pi N \tag{3}$$

where ξ_o = spatial frequency at which the spectrum is a maximum,

y_o = amount of horizontal shift in the signal,

λ_y = fringe line spacing, and

N = normalized fringe shift.

In this way the change in two raster lines is simply related to N. The difference between the phase for each raster line in the specimen and the average phase determined for the saline reference raster lines is simply $\Delta\phi(\xi_o)$. There is a 2π ambiguity problem inherent in determination of the phase using Fourier transforms, but it was solved using a phase unwrapping algorithm.

The accuracy of the SFDT was evaluated using simulated ideal sinusoids with noise added. Using a 32 point Fast Fourier Transform for sinusoids of 37 points gave an error of 0.016 for the determination of N, which is better than the earlier methods. The SFDT gave speed of sound results identical to those obtained using the previous automated spatial technique [23]. The SFDT also has several advantages over the previous method. It works for heterogeneous specimens, is twice as fast, is more noise tolerant, and analyzes the image in the vertical direction rather than horizontal, thereby giving 12 times more speed values per line analyzed. Still, a few modifications of the SFDT were introduced for wound healing studies in order to make the method more adaptable to the variations in the SLAM images.

The original method assumed the fringe line spacing (wavelength of the raster signal) was constant over the entire image and determined the phase at a fixed frequency. However, investigation of the digitized data for several interference images showed this was not the case. The saline image was found to have maximum frequency components between 700 and 800 kHz depending on the position in the image. In addition, the fringe line width and thus spacing is considerably more variable in the heterogeneous skin specimen. Here the raster lines had maximum frequency components between 600 and 800 kHz. As a result of these variations the Fourier Transform of the raster signal is computed for a range of frequencies in the modified technique, and the phase for the frequency with the maximum amplitude is used to compute N.

In the modified SFDT a Discrete Fourier Transform (DFT) is used to compute the frequency components. This allows the data window length to be an integer number of wavelengths, even for wavelengths which are not a power of two, thus reducing leakage in the Fourier Transform. A long DFT is used in order to make the frequency spacing smaller and the data are padded with zeroes if necessary. Also, since the raster signal is narrowband (600 -800 kHz), it is only necessary to compute a few of the frequency components of the DFT. The coefficients of these frequency components are precalculated and stored by the program in order to reduce computation time. The DFT length, frequency components computed, data window length, and position on the image are all program parameters which can be varied as desired. Typically, a

DFT length of 768, 18 frequency components between 600 and 915 kHz, and a window of 20 data points (the average raster signal wavelength of the system) are used to calculate N. It takes about 4 minutes to compute and plot one speed value for each raster line (for a total of 255), which is slightly faster than the unmodified SFDT.

An earlier study verified the validity of the SFDT [24]. The reproducibility of the speed measurements, calculated as the average absolute difference between each speed value and the mean speed value and expressed as a percentage of the mean value, is $\pm$ 0.4%. The sources of errors in the speed determination include the reference medium speed, the normalized fringe shift, the specimen thickness, and noise and other unknown system variations. If saline is used as the reference medium and the temperature at which the measurements are made is known ($30^{o}C$), the error due to the reference speed is minimal. The effect of an error in thickness on speed can be determined from Eq. (2) by varying T while keeping the other parameters constant. It was found that the error in speed measurements obtained using the modified SFDT is almost entirely due to errors in determining specimen thickness. The corresponding error in speed resulting from the $\pm$ 10% error in thickness measurement present is $\pm$ 3% to $\pm$ 1.3% for a speed range of 1550 to 1770 m/s.

3.4. Heterogeneity Index

The final measure used to assess wound status is a Heterogeneity Index (HI). The series IV study generated a crude HI for the first time [25]. That index took advantage of the fact that, by using the modified SFDT to determine the speed of sound in a specimen, many speed values, each representative of a different area of the specimen, are obtained. The variation in this spatial speed distribution was then used as an indication of the acoustic heterogeneity of the specimen. The standard deviation (SD) of the mean speed value gave a statistical measure of the variation of the speed values about the mean. The variation in speed in a specimen includes variation due to the SLAM system as well as variation due to the heterogeneity of the specimen. Consequently, the HI consisted of the speed variation in a specimen minus the variation due to the system. This measure of an HI proved not to be sensitive enough to reflect changes in the wound healing process. One of the main focuses of the current work then, was to develop a more sensitive measure of specimen heterogeneity.

The image processor was used exclusively to determine specimen heterogeneity. In addition, heterogeneity was measured using both the interference image and the acoustic image. A two dimensional velocity image is obtained from the interference image. The SFDT uses 20 data points horizontally for each speed value, corresponding to 39 horizontal pixels at 80 μm per pixel. Using 80 μm as the length of each vertical pixel as well corresponds to averaging ten velocity values in the vertical direction

for a given horizontal location. In this way, a 26 x 37 element two-dimensional image is generated and can be analyzed on the image processor. To generate a two dimensional acoustic image, the entire acoustic micrograph is digitized. For ease of comparison, this 255 x 768 point digitized image is converted into a 26 x 37 element image by simply averaging together the values in each corresponding block.

As mentioned earlier, the IIS image processor is supported by a DEC R SX11-M operating system. Before any processing could be done the two-dimensional image files had to be converted to a form compatible with this operating system. This was accomplished by first transferring the files from the VAX 11/730 to the Bioacoustics Research Laboratory's LS-11. The files were then transferred onto 7 1/4" floppy disks using the LS-11 system and taken to the Lab housing the image processor. The RSX11-M system set-up allowed the image files to be read in from these floppy disks.

After each image file had been read into the image processor, some rudimentary commands were performed to generate a measure of heterogeneity. Histogram equalization computes the histogram of the input image, then maps the pixel intensity levels such that the cumulative histogram of the output image is linear. This results in an image with fewer gray levels, since sparsely populated pixel intensity regions on the histogram are compressed, while densely populated regions are spread out. In this way the contrast is increased for densely populated intensity levels. By next using the Blotch function, it is possible to block off

different subregions of the image which are of interest, namely the specimen itself and the wound and skin areas within the specimen. Finally, the Statistics function produces a printout of summary statistics for the subregion(s) defined by BLOTCH. The contents include the following:

1. Number of pixels considered.
2. Minimum value of the pixels encountered.
3. Maximum value of the pixels encountered.
4. Mean value of the pixels.
5. Standard deviation of the pixels.
6. Mode of the pixels.
7. Median value of the Pixels.
8. Values of the three quartiles.
9. Values of the nine decimal.

The standard deviation of the pixels is then used as the heterogeneity index.

Statistics of a picture's gray levels are not generally useful as textural properties [26]. The gray level variance, for example, is the same for any two valued picture that has equal numbers of 1s and 0s whether the 1s are all in one half of the picture, in alternate rows, in a checkerboard pattern, or randomly distributed. Statistics of joint gray level occurrences, on the other hand, representing the frequencies with which various pairs of gray levels occur at neighboring point of the picture, do provide more useful textual information. However, this study is concerned only with determining a very rough measure of specimen heterogeneity and seeing if it is correlated with the

wound status. Future studies will most likely undertake more second order processing assuming heterogeneity proves to be a valuable parameter. Thus, first order statistics are sufficient for the present time.

3.5. Biochemical and Tensile Strength Determinations

One of the objectives of this wound healing study was to correlate the ultrasonic parameters, of speed, attenuation coefficient, and heterogeneity with the traditional biochemical measures of wound strength. However, the collagen content and tensile strength data were not available at the time this report was written. As a result, the correlation between acoustic properties and biochemical properties could not be examined.

3.6. Statistical Method

A repeated measures analysis of the data was performed using a standard statistical package, SPSS, available on the University of Illinois Cyber computer system. The SPSS package was specifically used for a multivariage analysis of variance [MANOVA].

CHAPTER 4

SERIES V RESULTS AND DISCUSSION

The series V experiments were done to verify the results of the series III and IV experiments and also to further explore the use of specimen heterogeneity in assessing wound status. Two dogs were included in the series V experiments. Wound specimens containing wound and adjacent skin, representing wound ages of 9, 20, 33, 49, 75, and 99 days, were analyzed. Perpendicular sections of wounded tissue were provided for each wound age along with control skin specimens obtained at least 2 cm away from the wound.

Ultrasonic attenuation coefficient, speed, and heterogeneity index were determined for the wound and adjacent skin areas of each wound specimen and for each control skin specimen. The ultrasonic results are presented in this chapter and are also summarized in Appendix I.

4.1. Experimental Observations

Figure 7 shows the SLAM optical, acoustic amplitude, and interference images obtained in a section containing a 20 day old wound. These images are representative of the wound specimens analyzed with the SLAM.

A number of observations can be readily made from the SLAM images. For early wounds such as these, the skin and wound areas are easily distinguished. In Figures 7a and 7b, the skin areas can be seen at the top and bottom of the specimen and the wound

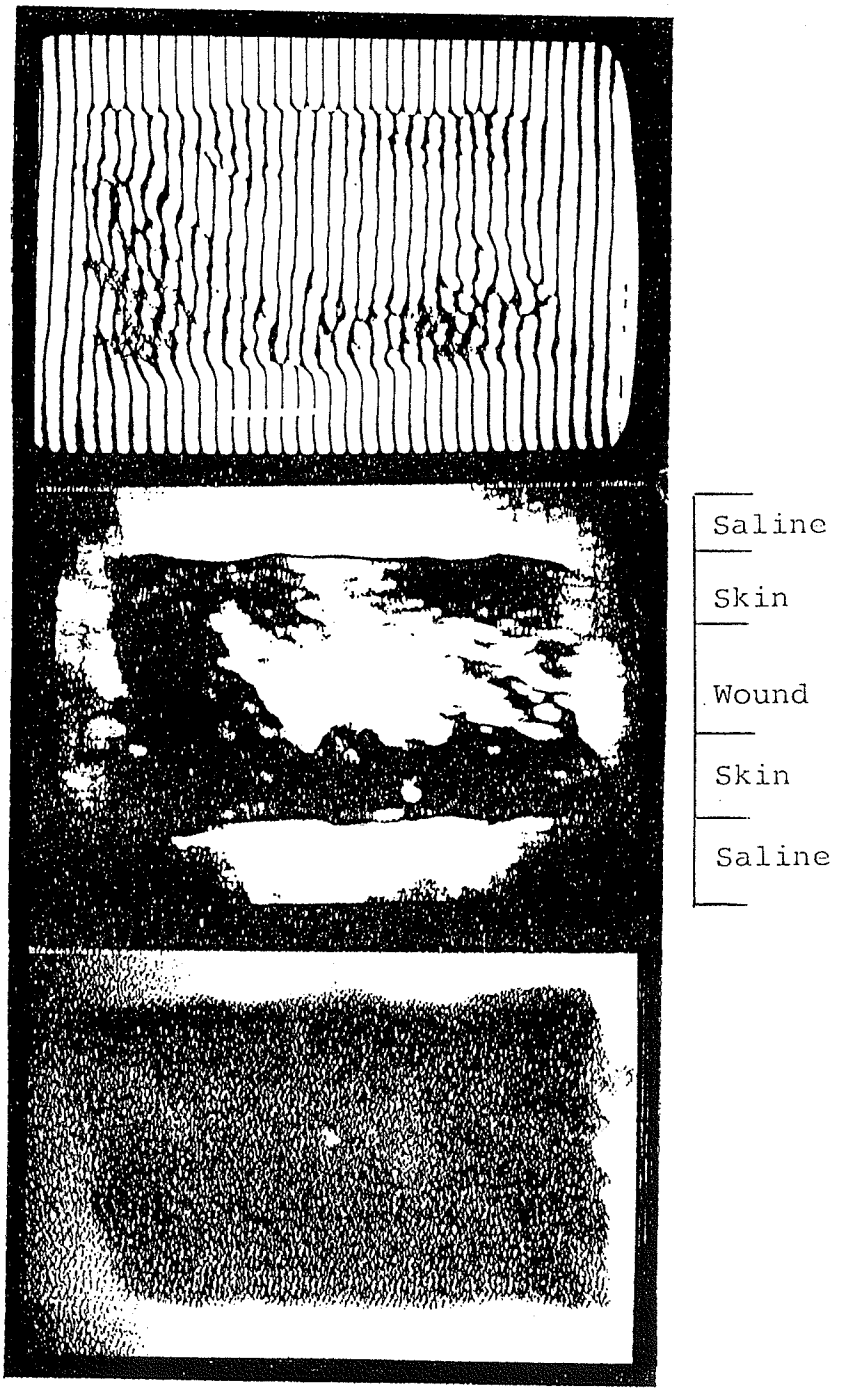

Figure 7 - (a) Interference, (b) acoustic amplitude, and (c) optical SLAM images for a 100 μm section with a 20 day old wound.

area is in the middle of the specimen. The optical image (Figure 7c) does not reflect this due to problems in obtaining a clear reproduction of a photograph of the monitor. The acoustic image shows the wound area to be much brighter than the adjacent skin, indicating the acoustic attenuation is lower in the wound. Also, the interference image shows the fringe shift of the interference lines to be greater in the skin than the wound, indicating the speed is greater in the skin. Not only is the fringe shift greater in the skin, but the lines are also much less uniform than in the wound, meaning the wound area is more homogeneous.

Later wounds were much more difficult to identify from the SLAM images. In these specimens the healing processes were so far advanced that the wound area was almost indistinguishable from the adjacent skin. Figures 8 and 9 illustrate how the healing process affects the speed measurements. Figure 8 shows a 20 day old wound. The skin and wound areas are easily discernable, with the speed being much lower in the wound than in the skin. Figure 9 shows a 49 day old wound specimen. The wound-skin interface is still identifiable, but the two regions are not nearly as distinct as before.

The make-up of the specimens also played a role in wound identification and data collection. The dogs examined in this study were very hairy and also had a thin epidermal layer. Both of these features caused some problems. Hair follicles caused discontinuities in the interference lines, giving inflated speed values, and they also increased the attenuation of the specimen.

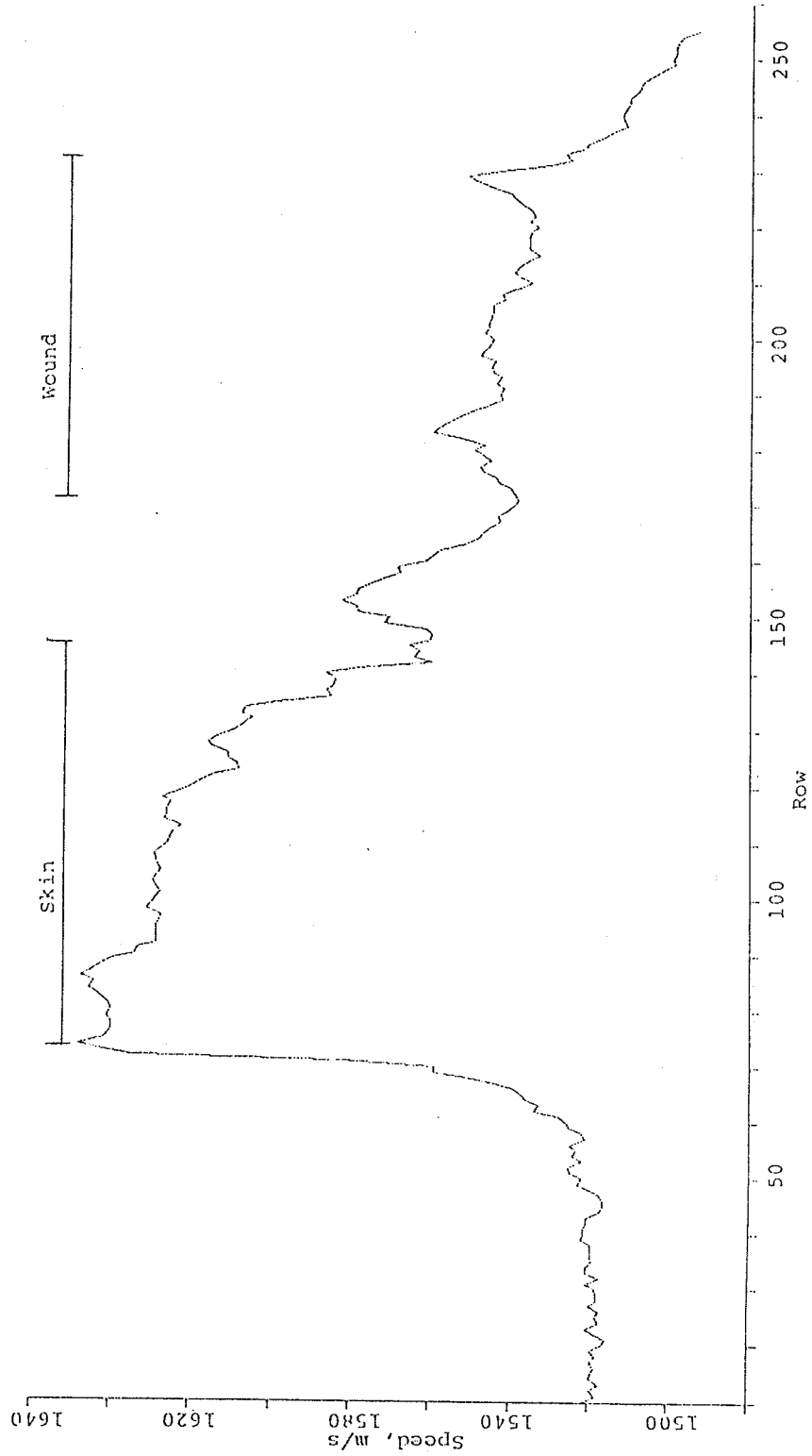

Figure 8 - Ultrasonic speed profile determined from the SLAM interference image for a 150 µm section with a 20 day old wound.

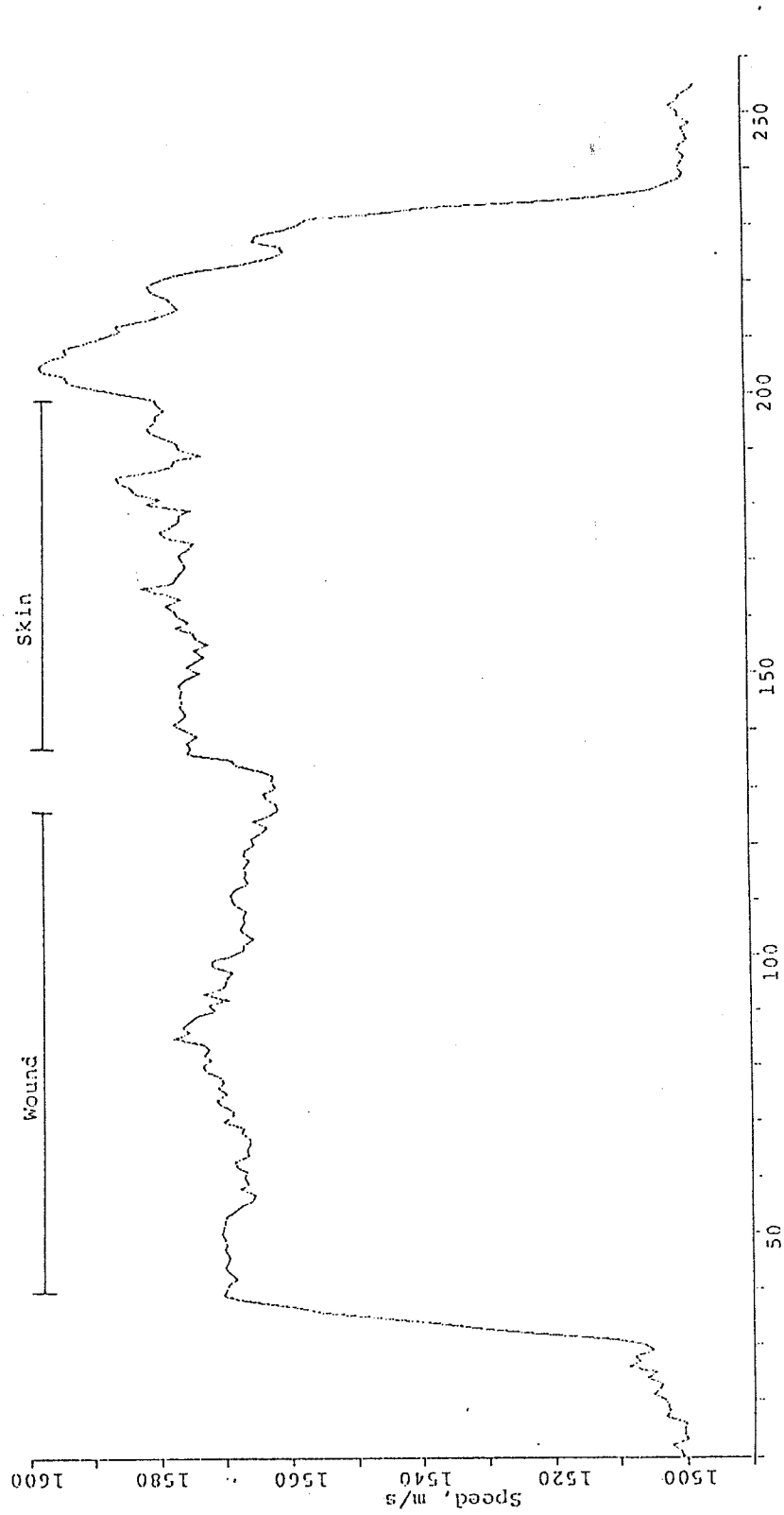

Figure 9 - Ultrasonic speed profile determined from the SLAM interference image for a 150 µm section with a 49 day old wound.

The only way to avoid these problems is to prepare the specimen such that as few hair follicles as possible are present. The epidermal layer meant each specimen contained a large portion of subcutaneous fat. This fat tissue also will produce distorted results. Speed values in fat are lower than skin and the attenuation is also much less. Again, the only way to avoid this is to carefully prepare each specimen. However, a large number of hair follicles and a large layer of fat were present in most specimens even after very careful preparation.

4.2. Ultrasound Results

A multivariate analysis of variance (MANOVA) was done on the ultrasonic speed, attenuation, and heterogeneity data to determine the effect of wound age, tissue type, and specimen thickness on the measurements. The effect of dog was not examined since only two dogs were involved in the study and did not provide a large enough population. Table 1 lists the factors and categories used on the MANOVA.

The MANOVA results showed that age and tissue type had a significant effect on the ultrasonic data but the specimen thickness did not. For this reason the three different values of speed for each specimen were combined and the mean was used. The heterogeneity data was reduced in a similar fashion. Changes in the ultrasonic parameters in the skin and wound were examined by plotting attenuation coefficient, speed, and heterogeneity as a function of wound age. Separate plots are drawn for each dog.

Table 1. Factors and Categories Included in the MANOVA for Series V Data.

FACTORS	CATEGORIES
Dog	1) A 2) B
Wound Age (days)	1) 9 2) 20 3) 33 4) 49 5) 75 6) 99
Thickness (m)	1) 75 2) 100 3) 150
Tissue	1) skin 2) wound 3) control

Figures 10, 11, and 12 show the speed, attenuation coefficient, and heterogeneity as a function of wound age for dogs A and B. For dog A (Figure 10) both speed and attenuation coefficient were lower in the wound than in the skin. The speed was also generally lower in the adjacent skin than the control skin. However, the attenuation did not show the same difference in speed between the adjacent skin and the contrast skin. In dog B (Figure 11), the speed and attenuation were lower in the wound than in the adjacent skin. Also, speed and attenuation were lower in the adjacent skin than in the control skin except for the attenuation at day 75, which was lower in the control skin than in the adjacent skin. Heterogeneity (Figure 12), was a little more difficult to classify. In dog A wound heterogeneity was lower than in the adjacent skin except at day 20. Also, heterogeneity was

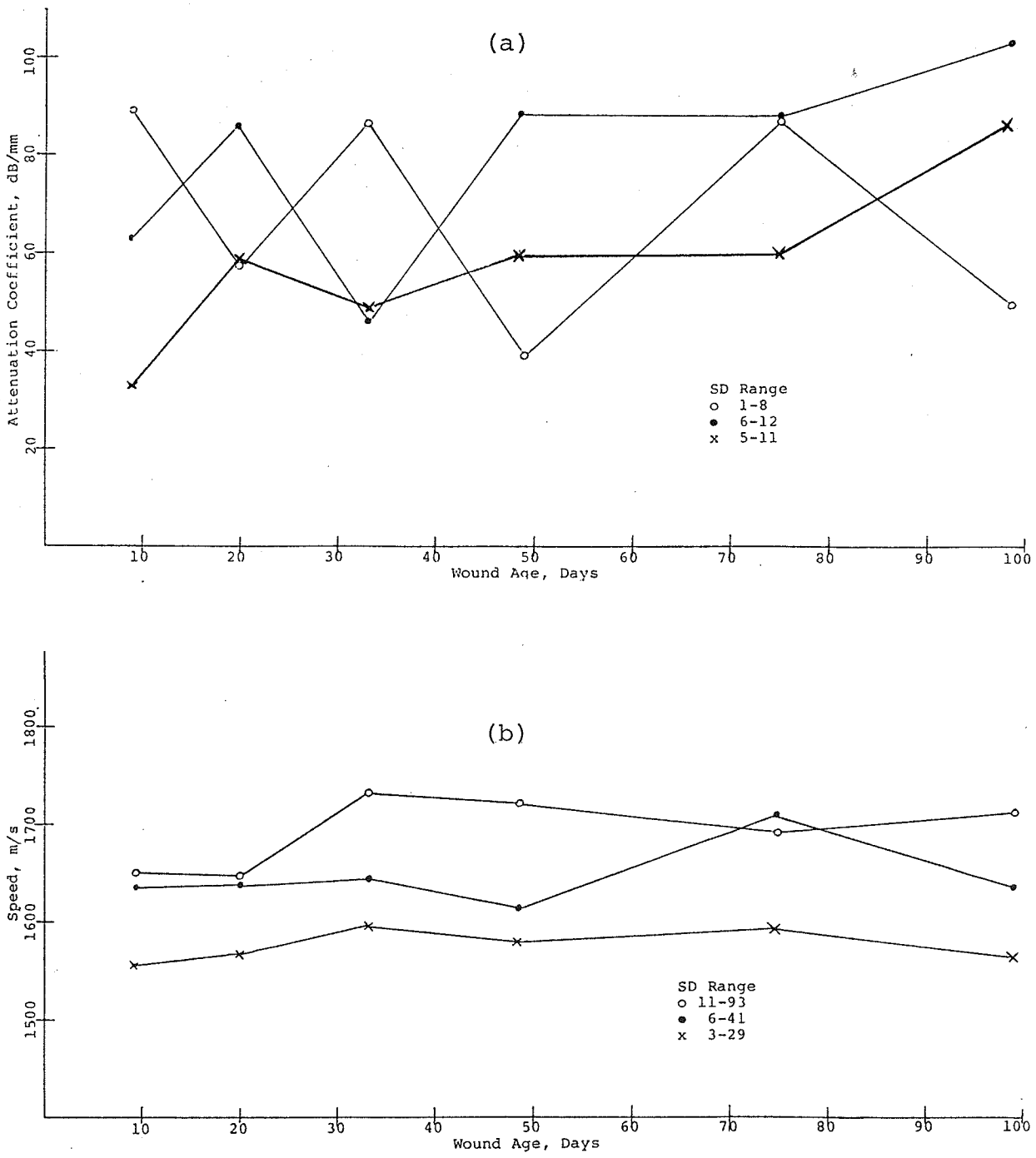

Figure 10 - Attenuation coefficient (a) and ultrasonic speed (b) versus wound age for control skin (o), adjacent skin (•), and wound (×) for dog A.

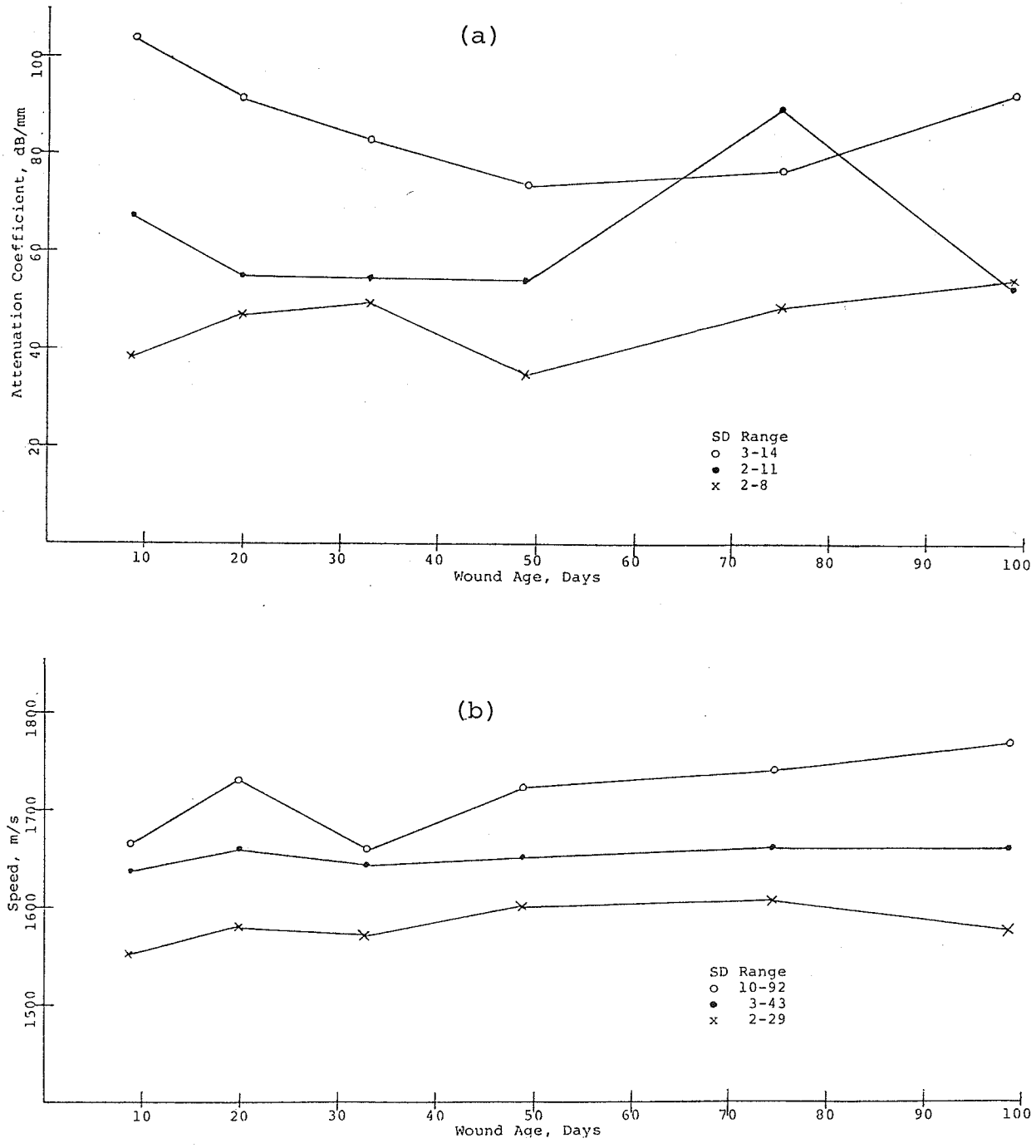

Figure 11 - Attenuation coefficient (a) and ultrasonic speed (b) versus wound age for control skin (o), adjacent skin (•), and wound (x) for dog B.

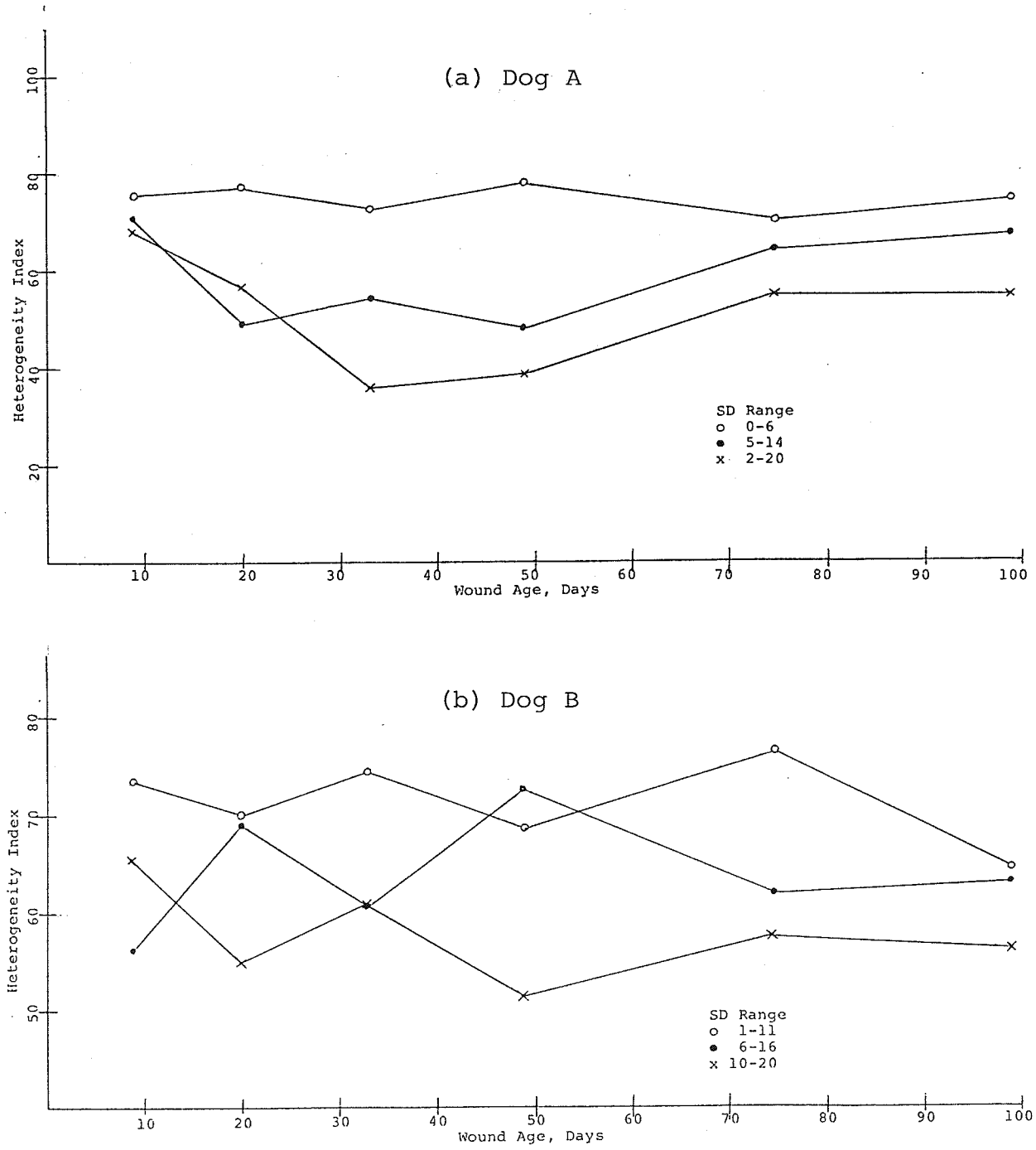

Figure 12 - Heterogeneity index versus wound age for control skin (o), adjacent skin (•), and wound (×) for dog A (a) and dog B (b).

lower in the adjacent skin than in the control skin. Dog B, however, was slightly different. Wound heterogeneity was lower than the adjacent skin except at nine and 33 days, and adjacent skin heterogeneity was lower than control skin except at day 49. The overall trend seems to be that the ultrasonic parameters are lowest in the wound area and highest in the control skin with values for the adjacent skin lying somewhere in between.

The MANOVA results predicted the variation due to tissue type is much greater than that due to wound age, and this is seen to be the case. While it was fairly easy to classify the ultrasonic parameters according to tissue type, regular variations with age are harder to spot. Dog A wound tissue speed increases until day 33 but then decreases slightly. The adjacent skin is somewhat similar. The speed stays fairly constant, increases at day 75, but then decreases again at day 99. Dog B speed exhibits much of the same behavior. The wound velocity increases until day 49, levels off through day 75, and then decreases slightly at day 99. The adjacent skin increases slightly at day 20, decreases again at day 33, and then stays essentially the same.

The attenuation results are also marked by the lack of any real trend with age. Dog A attenuation increases from day nine to day 20, decreases from day 20 to day 33, increases again at day 49, stays fairly constant to day 75, and increases once more at day 99 for both wound tissue and the adjacent skin. The dog B attenuation is not nearly as correlated. For the wound tissue attenuation increases from day 9 to day 20, decreases from day 33 to day 49, and then steadily increases to day 99. The adjacent

skin attenuation decreases from day nine to day 20, remains constant to day 49, increases at day 75, and then decreases at day 99.

Ultrasonic heterogeneity is shown in Figure 12. Wound and adjacent skin values show essentially the same trend. There is a decrease in the heterogeneity from day nine to day 33, and then it increases again until day 99. The dog B heterogeneity data shows more oscillations. The wound heterogeneity decreases from day nine to day 20, increases from day 20 to day 33, decreases from day 33 to day 49, increases from day 49 to day 75, and finally decreases again to day 99. The adjacent skin also alternates increasing and decreasing over the entire range of ages.

As mentioned earlier, the control skin represents skin specimens evenly spaced from the head to the tail of the dog, with day nine near the head and day 99 near the tail. For both dogs the ultrasonic speed ends up being slightly greater at the tail than at the head. However, there are random variations of the speed values in between the two ends. The attenuation does not exhibit any consistent trend either. For dog A the attenuation alternates decreasing and increasing from the head down to the tail. In dog B the attenuation steadily decreases until midway down the dog, and then steadily increases until reaching the tail. For the heterogeneity index both dogs exhibit values which alternate decreasing and increasing from head to tail. No pattern exits for these seeming random variations. Tables 2 and 3 list the speed and attenuation values, respectively, of the con-

trol skin. The average speed value for all 12 control specimens is 1703 ± 35 m/s. This value compares favorably to the values of 1633 ± 40 m/s found earlier for dog skin at 100 MHz [1]. The average attenuation coefficient is 79 ± 20 dB/mm, which also compares to the value of 57 ± 10 dB/mm found in a previous study [1].

Table 2. Ultrasonic Speed in Normal Dog Skin from Six Locations (I to VI Represent Locations from Head to Tail Along Back).

	SPEED, M/S					
	I	II	III	IV	V	VI
Dog A	1653	1647	1727	1721	1692	1715
Dog B	1664	1720	1659	1723	1738	1764

Table 3. Ultrasonic Attenuation Coefficient in Normal Dog Skin from Six Locations (I to IV Represent Locations from Head to Tail Along the Back).

	SPEED, M/S					
	I	II	III	IV	V	VI
Dog A	89	58	87	39	86	49
Dog B	105	93	84	74	77	94

CHAPTER 5

SUMMARY AND CONCLUSIONS

Ultrasonic speed, attenuation coefficient, and heterogeneity index were measured in dog skin and wound tissue using the 100 MHz SLAM. Perpendicular sections, representing wound ages from nine to 99 days, and six locations along the back of the dog from a total of two dogs were evaluated.

5.1 Ultrasound Results

1. The ultrasonic speed and attenuation coefficient were generally lower in the wound than in the adjacent skin. They also increased with increasing wound age with the largest increase in speed being about 2% and the largest increase in attenuation being about 75%. The wound and adjacent skin profiles usually paralleled one another.
2. The control skin specimens exhibited no consistent pattern in the variations of the speed and attenuation coefficients. The average speed value of 36 specimens was 1703 $\pm$ 40 m/s, while the average attenuation coefficient was 78 $\pm$ 20 dB/mm. These values are slightly higher than previously reported values, but that is most likely due to the high number of hair follicles present in these dogs.
3. The heterogeneity index was also generally lower in the wound skin than in the adjacent skin, and the profiles of the two regions were fairly similar. However, no conclu-

sions could be drawn about trends occurring as a function of wound age. The results were too scattered.

5.2. Conclusions

1. Ultrasonic speed, attenuation coefficient, and heterogeneity index are different in the wound than in the skin, and change as a function of wound age.
2. The ultrasonic parameters vary randomly in control skin according to location on the dog.
3. The heterogeneity index was generally lower in the wound than in the skin, but was not accurate enough to reflect changes as a function of wound age.
4. More work needs to be done using the image processor to establish a sensitive, accurate heterogeneity index. The present images used are much too coarse.

APPENDIX I:

ULTRASONIC SPEED, ATTENUATION COEFFICIENT, AND HETEROGENEITY INDEX (HI) FOR SERIES V

For the control skin the specimen are equally spaced along the back of the dog from head to tail. The nine day sample was near the head, and the 99 day sample was near the tail. The speed value and HI listed are the averages of the values for three thicknesses.

DOG	WOUND AGE	SPEED (m/s)	ATTENUATION COEFFICIENT (dB/mm)	HI
		CONTROL SKIN		
A	9	1653	89.3	76
	20	1647	57.7	78
	33	1727	86.6	73
	49	1721	39.1	78
	75	1692	86.3	71
	99	1715	49.2	76
B	9	1664	105.1	74
	20	1720	92.8	70
	33	1659	83,9	74
	49	1723	74.1	69
	75	1738	77.0	77
	99	1764	93.5	65

DOG	WOUND AGE	SPEED (m/s)	ATTENUATION COEFFICIENT (dB/mm)	HI
		ADJACENT SKIN		
A	9	1653	63.8	71
	20	1647	86.0	50
	33	1727	46.3	54
	49	1721	88.4	48
	75	1692	87.2	65
	99	1715	107.4	68
B	9	1638	67.1	56
	20	1660	54.9	69
	33	1644	56.5	61
	49	1647	54.7	73
	75	1659	90.5	62
	99	1657	53.0	63

DOG	WOUND AGE	SPEED (m/s)	ATTENUATION COEFFICIENT (dB/mm)	HI
		WOUND		
A	9	1555	32/0	68
	20	1566	58.2	58
	33	1595	47.7	36
	49	1580	59.4	39
	75	1591	59.2	55
	99	1561	183.8	56
B	9	1555	38.3	66
	20	1581	47.1	55
	33	1577	49.7	61
	49	1599	34.6	52
	75	1601	49.0	58
	99	1572	54.1	57

REFERENCES

1. Steiger, D., "Ultrasonic Assessment of Skin and Wounds with the Scanning Laser Acoustic Microscope," M.S. Thesis, Department of electrical Engineering, University of Illinois, Urbana-Champaign, IL, 1986.

2. O'Brien, W. D., Jr., Olerud, J., Shung, K. K., and Reid, J. M., "Quantitative acoustical assessment of wound maturation with acoustic microscopy," JASA, Vol. 69, pp. 575-579, 1981.

3. O'Brien, W. D., Jr., "The role of collagen in determining ultrasonic propagation properties in tissue," Acoustical Holography, L. W. Kessler, Editor, Vol. 7, Plenum Press, New York, pp. 37-50, 1977.

4. Peacock, E. E. and Van Winkle, W., Jr., "The biochemistry and the environment of wounds and their relation to wound strength," Surgery and Biology of Wound Repair. W. B. Saunders Co., Philadelphia, PA, pp. 129-169, 1970.

5. Schilling, J. A., "Wound healing," Surgical Clinics of North America, Vol. 56, pp. 859-874, 1976.

6. Peacock, E. E., Jr. and Van Winkle, W., Jr., "Structures, synthesis, and interaction of fibrous protein and matrix," Surgery and Biology of Wound Repair. W. B. Saunders Co., Philadelphia, PA, pp. 75-127, 1970.

7. Dunn, F., "Ultrasonic properties of biological media," in Ultrasound Interactions in Biology and Medicine, R. Millner, E. Rosenfeld, and J. Cobet, Editors. Plenum Publishing Corp., pp. 1-6, 1983.

8. Goss, S. A. and Dunn, F., "Ultrasonic propagation properties of collagen," Physical Medicine and Biology, Vol. 25, pp. 827-837, 1980.

9. Fields, S. and Dunn, F., "Correlation of echographic visualizability of tissue with biological composition and physiological state," JASA, Vol. 54, pp. 809-812, 1973.

10. Johnston, R. L., Goss, S. A., Maynard, V. A., Brady, J. K., Frizzell, L. A., O'Brien, W. D., Jr., and Dunn, F, "Elements of tissue characterization. Part I. ultrasonic propagation properties," Ultrasonic tissue Characterization II, M. Linzer, Editor. National Bureau of Standards, Special Publication 525, U.S. Government Printing Office, Washington, DC, pp. 19-27, 1979.

11. O'Brien, W. D., Jr., "The relationship between collagen and ultrasonic attenuation and velocity in tissue," Ultrasonics International 1977, Conference Proceedings. IPE Business Press Limited, England, pp. 194-205, 1977.

12. Owner's Manual Sonomicroscope-System 140 Scanning Laser Acoustic Microscope. Sonoscan, Inc., Bensenville, IL, 1983.

13. Foster, S., "An Image Digitizing System for A Scanning Laser Acoustic Microscope," M.S. Thesis, Department of Electrical Engineering, University of Illinois, Urbana-Champaign, IL, 1981.

14. Embree, P. M., Foster, S. G., Bright, G., and O'Brien, W. D., Jr., "Ultrasonic velocity spatial distribution analysis of biological materials with the scanning laser acoustic

microscope," Acoustical Imaging, M. Kaveh, R. K. Mueller, and J. F. Greenleaf, Editors, Vol. 13, Plenum Press, New York, pp. 203-216, 1984.

15. Olerud, J., O'Brien, W. D., Jr., Henderson, M. A. R., Steiger, D. L., Forster, F. K., Daly, C., Ketterer, D., and Odland, G. F., "Ultrasonic assessment of skin and wounds with the scanning laser acoustic microscope. Journal of Investigative Dermatology," (in press).

16. Tervola, K. M. U., Foster, S. G., and O'Brien, W. D., Jr. "Attenuation coefficient measurement technique at 100 MHz with the scanning laser acoustic microscope," IEEE Transactions on Sonics and Ultrasonics, Vol. SU-32, No. 2, pp. 259-265, March 1985.

17. Tervola, K. M. U. and O'Brien, W. D., Jr., "Spatial frequency domain techniques: an approach for analyzing the scanning laser acoustic microscope interferogram images," IEEE Transactions on Sonics and Ultrasonics, Vol. SU-36, No. 4, pp. 544-554, July 1985.

18. Embree, P. M., Tervola, K. M. U., Foster, S. G., and O'Brien, W. D., Jr., "Spatial distribution of the speed of sound in biological materials with the scanning laser acoustic microscope," IEEE Transactions on Sonics and Ultrasonics, Vol. SU-32, pp. 341-350, 1985.

19. Rosenfeld, A. and Kak, A. Digital Picture Processing, Academic Press, New York, pp. 418-425, 1976.